ELSEVIER

Journal of Structural Geology 27 (2005) 23–34

JOURNAL OF STRUCTURAL GEOLOGY

www.elsevier.com/locate/jsg

Extensional fault arrays in strike-slip and transtension

John W.F. Waldron*

Department of Earth and Atmospheric Sciences, 1-26 ESB, University of Alberta, Edmonton, Alberta, Canada T6G 2E3

Received 1 January 2004; received in revised form 3 June 2004; accepted 30 June 2004
Available online 13 October 2004

Abstract

Sedimentary basins developed under conditions of strike-slip or transtension are subject to significant rotational strains, yet faults developed in such regimes are commonly explained using simplified models that ignore rotation. The heaves of extensional faults developed provide a means of quantifying this rotation. For ideal strike-slip (simple shear), the apparent stretch due to fault heaves can be related simply to shear strain. At shear strains (γ) above 1.0, previously formed extensional faults begin to show inversion as reverse faults, becoming fully inverted at $\gamma = 2.0$. In transtensional basins, the apparent stretch is related, in addition, to the initial orientation of the faults, which may itself be related to the incremental strain. In the Stellarton basin of Nova Scotia, Canada, fault heaves and orientations can be measured from subsurface mine plans. Measurements of these quantities indicate that strain was only mildly transtensional, with a small ($<10°$) angle of divergence (α). The measurement of fault heaves potentially provides detailed information on strain wherever strike-slip or transtensional basins have been explored in detail by seismic or other subsurface methods.

Keywords: Kinematics; Strike-slip; Transtension; Fault; Strain; Pull-apart basin

1. Introduction

Sedimentary basins developed in strike-slip settings are subject to deformation from the earliest stages of basin development. However, many analyses of the geometrical features of such basins have been based on, and limited by, hypothetical orientations of stress axes, and infinitesimal strains (e.g. Fig. 1a). Such models neglect the effects of incremental rotations in progressive strain (illustrated schematically for simple shear in Fig. 1b and c). In contrast, kinematic analyses of thrust belts and rifts have focussed on the development and effect of features that involve significant rotations during progressive strain, such as thrust duplexes and listric extensional growth faults. Thus, progressive deformation of sedimentary rocks in these settings is relatively well understood. The effects of rotational strain in strike-slip basins have been relatively neglected, probably because this deformation inevitably involves large departures from plane strain, and is therefore harder to handle geometrically.

This paper develops a simple kinematic model for the deformation of a sedimentary basin in a strike-slip setting, where extension is manifested in the development of normal faults. The model is based in part on structures mapped in the subsurface of the coal-bearing Stellarton Basin (Fig. 2) in the Carboniferous of Nova Scotia, in the Appalachians of eastern Canada (Waldron, 2004). Published descriptions of other strike-slip basins (Fig. 3) suggest that extensional faults are common, and therefore that the kinematic analysis applied to the Stellarton example is applicable to many other basins developed in comparable settings.

2. Fault arrays in strike-slip and transtensional basins

2.1. Kinematic styles of basin deformation

Fault arrays are common in basins developed in strike-slip and transtensional settings. In some cases the intra-basinal faults are predominantly strike-slip, with rotation of fault blocks about vertical axes in strike-slip duplexes (Woodcock and Fischer, 1986) and similar configurations; Fig. 4a shows one such kinematic style, based on figures by Dibblee (1977),

* Corresponding author. Tel.: +1-780-492-3892; fax: +1-780-492-2030
E-mail address: john.waldron@ualberta.ca.

0191-8141/$ - see front matter © 2004 Elsevier Ltd. All rights reserved.
doi:10.1016/j.jsg.2004.06.015

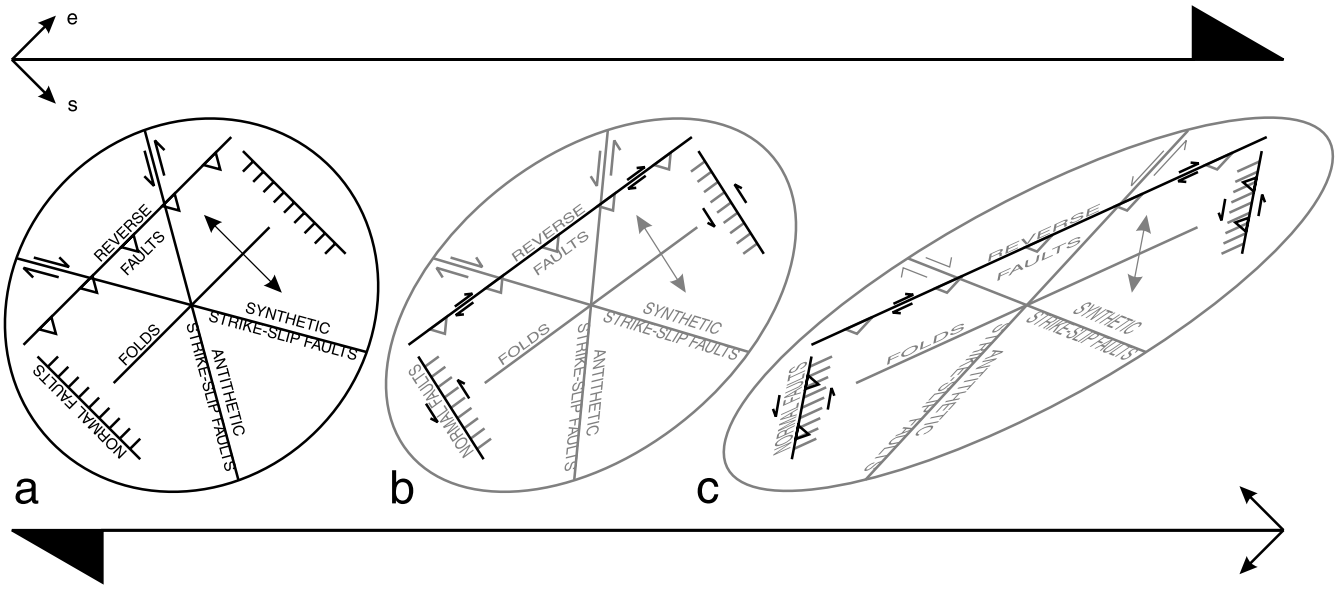

Fig. 1. (a) Diagram illustrating incremental strain associated with simple-shear deformation in a strike-slip zone, after Harding (1974). (b) Modification of (a) by continued simple shear, showing that previous (grey) normal and thrust faults acquire oblique slip (black). (c) Continued shear leads to inversion (black) of previous (grey) normal faults.

and Christie-Blick and Biddle (1985). For example, kinematic models proposed for the Mojave Desert and other basins related to the San Andreas fault (e.g. Garfunkel, 1974; Garfunkel and Ron, 1985; Dokka et al., 1998) are dominated by vertical rotations, in some cases documented with extensive paleomagnetic evidence. However, in many examples, faults with extensional, normal-sense slip are dominant within a basin, typically in an en échelon arrangement (Fig. 4b). This type of behaviour is here termed extension-dominated. Allen et al. (1998) have noted that significant rotations must occur under these circumstances also, on both horizontal and vertical axes, as shown in Fig. 4b. However, the relationship between rotation and the overall deformation environment has not been quantified.

A simple comparison of the bulk strain involved in the two styles suggests that extension-dominated basins should prevail in transtensional settings, because they produce a significant increase in basin-area, whereas wrench-dominated basins probably represent bulk strains that more closely approximate ideal strike-slip. A third, thrust-dominated style, would be anticipated in transpressional settings (e.g. positive flower-structures) where a significant amount of vertical extension occurs.

2.2. Characteristics of extension dominated basins

Arrays of normal faults in natural sedimentary basins deformed in strike-slip settings have been described by many authors (Harding, 1974; Dibblee, 1977; Aydin and Nur, 1985; Cemen et al., 1985; Harding et al., 1985; Wood et al., 1994; Allen et al., 1998). There is significant variation in the fault orientation both within and between basins; in many cases, fault orientations depart significantly from the orientations predicted by Fig. 1a. For example, Rodgers (1980) identified a small basin on the San Jacinto fault where normal faults are almost perpendicular to bounding strike-slip faults (Fig. 3). There are of course several possible explanations for this variation. Pre-existing basement features, or earlier strike-slip faults, may control the orientation of normal faults. Normal faults may develop during fault propagation, at fault tips, which are areas of inhomogeneous stress and strain. Also, basins may depart from the ideal of simple shear illustrated by Fig. 1; transtensional and transpressional strains will produce different initial fault orientations. Finally, progressive strain is likely to change the initial orientations of faults, either by rotation as shown in Fig. 1b and c, or by folding. Many of these effects can be seen in analogue models (Dooley and McClay, 1997; Rahe et al., 1998; Sims et al., 1999), in which normal faults are initiated in variable orientations and undergo rotation in the sense shown in Fig. 1.

The Pennsylvanian Stellarton basin of Nova Scotia (Yeo and Gao, 1987; Waldron, 2004) is interpreted as a pull-apart basin developed at the dextral Cobequid–Hollow fault

Fig. 2. Extensional faults in the Stellarton basin, Nova Scotia. (a) Simplified map of Stellarton basin showing location of underground coal mine data and subsurface fault traces (after Waldron, 2004). Insets show location in Nova Scotia of Stellarton basin and major Carboniferous fault zones: CCFZ = Cobequid–Chedabucto Fault Zone; HFZ = Hollow Fault Zone. (b) Enlarged structure contour map of subsurface Foord coal seam and faults that cut it. Contours are derived from original mine plans (hence depths in feet below sea level) as described by Waldron (2004). Cross-sections A–A′ to E–E′ show deformation of Foord seam by folds and faults. Location ticks show UTM (Universal Transverse Mercator) grid coordinates.

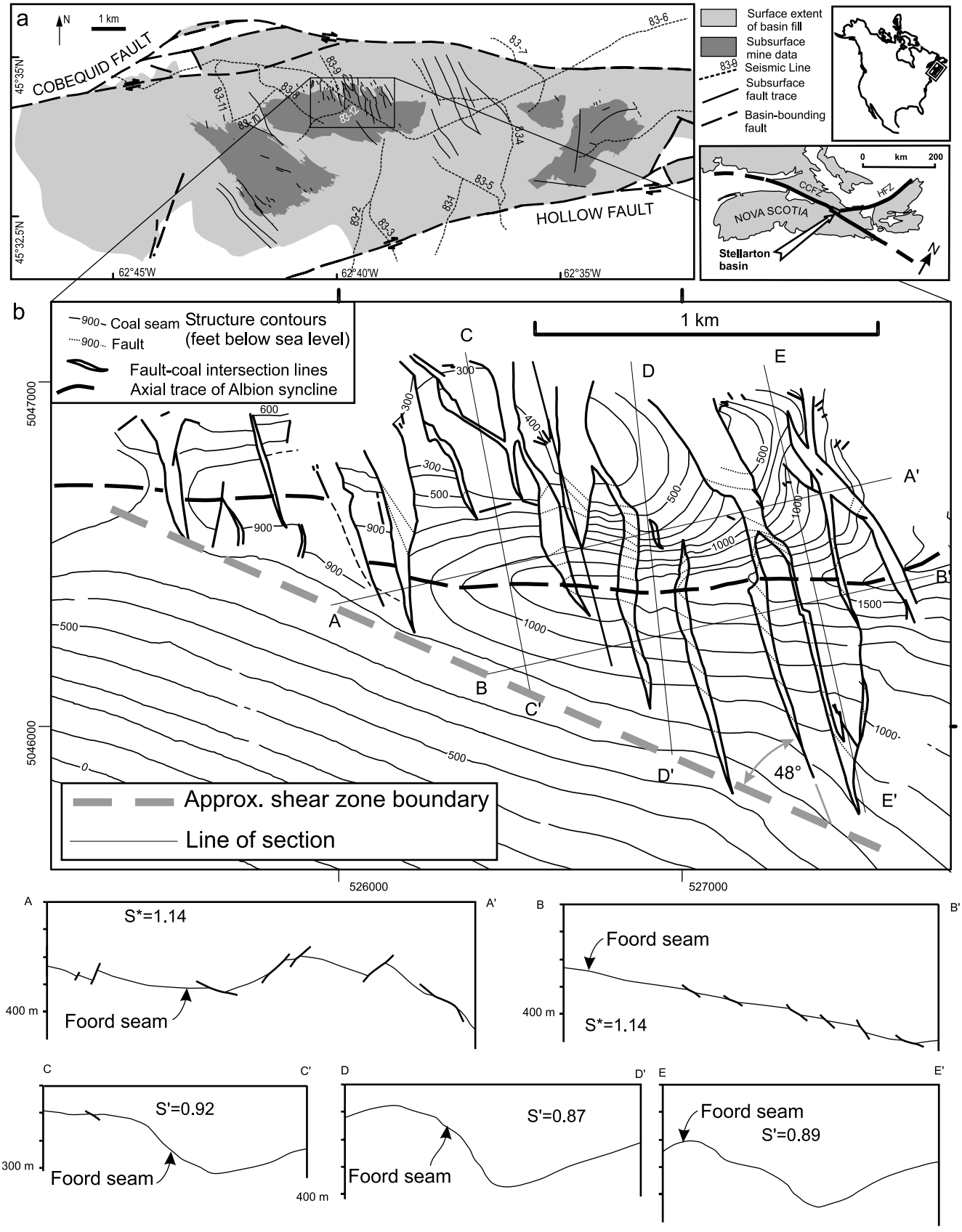
a
N
1 km
COBEQUID FAULT
HOLLOW FAULT
45°35'N
45°32.5'N
62°45'W
62°40'W
62°35'W
83-1
83-2
83-3
83-4
83-5
83-6
83-7
83-8
83-9
83-10
83-11
83-12
Surface extent of basin fill
Subsurface mine data
Seismic Line
Subsurface fault trace
Basin-bounding fault
0 km 200
CCFZ
HFZ
NOVA SCOTIA
Stellarton basin
b
900 Coal seam
900 Fault
Structure contours (feet below sea level)
Fault-coal intersection lines
Axial trace of Albion syncline
1 km
5047000
5046000
526000
527000
A
A'
B
B'
C
C'
D
D'
E
E'
48°
Approx. shear zone boundary
Line of section
S*=1.14
Foord seam
400 m
S'=0.92
300 m
S'=0.87
S'=0.89

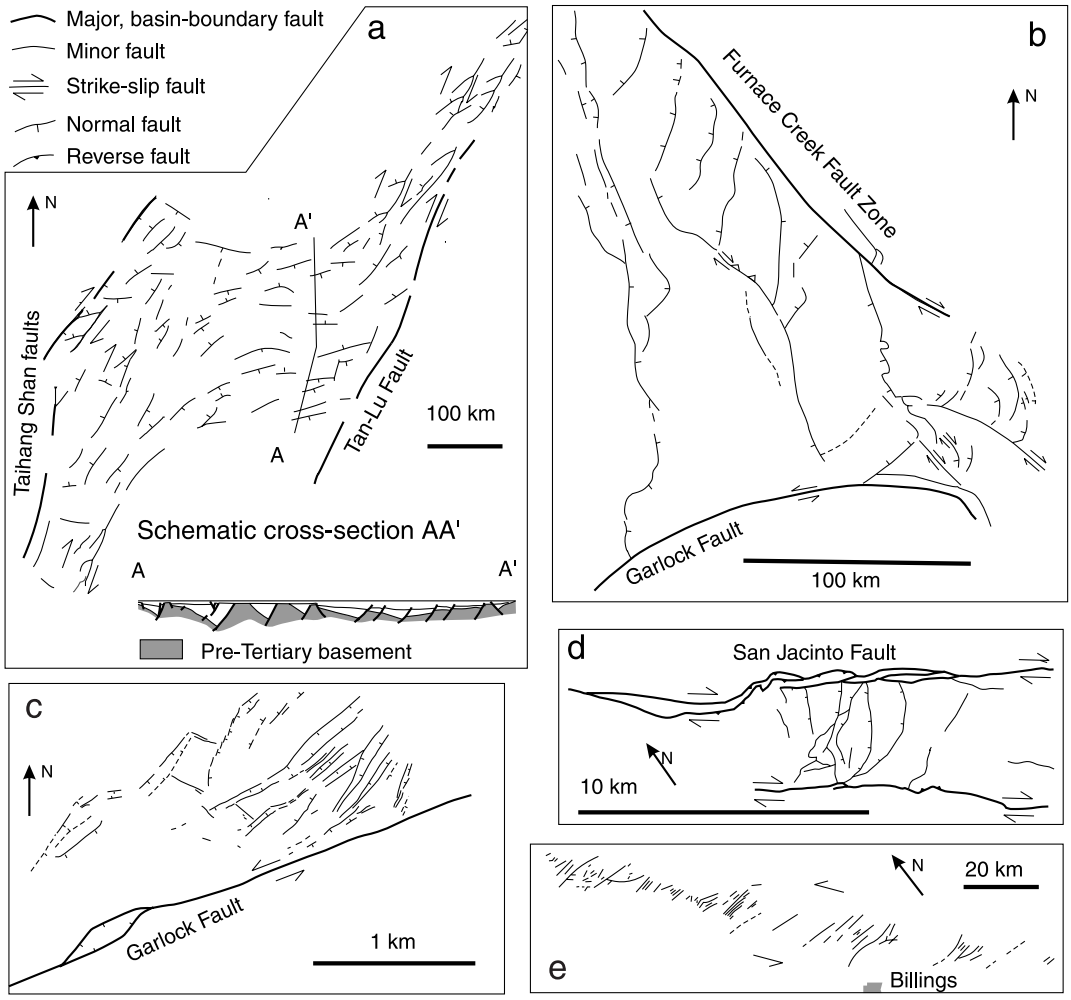

Fig. 3. Published examples of transtensional and strike-slip basins. (a) Bohai Basin, China (after Dokka et al., 1998). (b) Death Valley area (Cemen et al., 1985). (c) Cantil Valley adjacent to Garlock Fault, California (Aydin and Nur, 1985). (d) Basin on San Jacinto fault (Rodgers, 1980). (e) Sinistral fault zone at Billings, Montana (Harding et al., 1985).

system (Fig. 2). The basin contains numerous thick coal seams for which mine plans provide detailed information on subsurface geometry (Fig. 2b), allowing faults to be mapped in the subsurface. The Foord seam, the thickest and most extensively mined, shows a family of N–S to NNW–SSE-trending fault intersections. The horizontal component of offset, or heave, of a fault can in some cases be measured directly from annotations in the mine plans; in other cases the heave can be readily inferred from the pattern of mining. The fault heaves typically increase northward, and the trends of fault–coal intersections show small variations, interpreted to reflect mainly the rotation of faults and intervening blocks, but also showing effects of folding. The Albion syncline (Fig. 2b) is shown (Waldron, 2004) to fold both the coal seams and the faults, but the right-stepping character of the syncline across several faults shows that the faults continued to be active during folding.

If, as seems likely, the faulting of the Foord seam developed during dextral strike-slip or transtensional deformation of the basin fill, then there must be a relationship between the strain, the orientation of the faults, and the fault heaves. The results given in the following sections arose from an effort to determine this relationship for the Stellarton basin, but they can be generalized to all basins where strike-slip deformation is accommodated by slip on multiple normal faults.

3. Kinematic model for ideal strike-slip

In developing a model for the accommodation of transtension by en échelon normal faults, it is convenient to begin by considering the special case of simple shear parallel to vertical planar bounding surfaces, i.e. an ideal strike-slip setting. Later sections will generalize this special case to transtensional zones, in which a component of divergence is combined with strike-slip. Most of the conclusions could also be generalized to the transpressional case, although significant basin subsidence is less likely in transpressional settings.

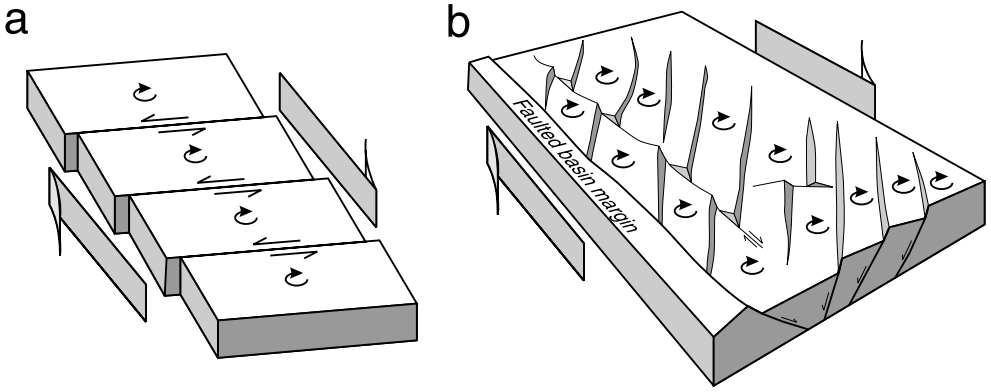

Fig. 4. (a) Wrench dominated block faulting in a zone of overall strike-slip, based loosely on illustrations by Dibblee (1977), Christie-Blick and Biddle (1985), and Dokka et al. (1998). (b) Extension dominated block faulting, modified from Allen et al. (1998), based on example from Bohai Basin, China.

3.1. General theoretical considerations

The infinitesimal strain, and by implication the stress, in an idealized homogeneous body of rock in a strike-slip setting can be represented as shown in Fig. 1a, based on many examples from the published literature (e.g. Harding et al., 1985). (For convenience, all examples are drawn for dextral motion.) For infinitesimal simple shear, the shear zone boundary is a line of no extension. Extensional structures (such as boudins and normal faults) and shortening structures (such as thrust faults and folds) are predicted to develop in orientations at 45° to the shear zone boundary, consistent with inferred directions of instantaneous shortening and extension.

When finite strain is considered, this model is complicated by rotation. Normal faults initiated in the positions shown in Fig. 1a are expected to rotate clockwise, moving into orientations where they may be expected to acquire strike-slip components of motion, synthetic to the sense of the main shear zone in the case of rotated thrust faults, and antithetic for rotated normal faults (Fig. 1b). Eventually, if the angle of shear ψ exceeds 45°, the normal faults may rotate through an orientation perpendicular to the shear zone boundary; beyond this point they would experience incremental shortening, and therefore would be expected to develop reverse slip (Fig. 1c). Geological consequences might include the development of inversion structures.

The following discussion considers the simple case of a basin in which the extensional component of simple shear is accommodated by faults, but the shortening component is accommodated by more ductile deformation, typically folding. This is an idealized model; in reality, progressive general shear is likely to result in the folding of faults soon after their initiation (Dewey, 2002). However, in the Stellarton basin of Nova Scotia, where such folding is easily demonstrated from contoured plans of mining operations (Waldron, 2004), faults can also be shown to have continued to slip during folding, because they serve to link folds that are offset en échelon. Hence, it is here assumed that extensional faults are able to continue to slip, concurrently with gentle to open folding or penetrative ductile strain that accommodates the shortening component of deformation.

3.2. Relationship of folds and faults to strain

To investigate and quantify the bulk strain, and particularly the finite rotation, implied by faults and folds having the style shown in Figs. 2 and 3, it is helpful to use a simplified conceptual model as indicated in Fig. 5. This model considers only the plan view of a stratum, and therefore emphasizes the effects of rotation about a vertical axis. The initial configuration represents a portion of basin in plan view as a square. Upon initiation of simple shear measured by $\gamma = \tan(\psi)$, extensional faults are initiated with strikes perpendicular to instantaneous extension at 45° to the shear zone boundary. It is assumed that the fault-bounded segments of width w rotate rigidly as if pinned to passive markers at the shear zone boundaries. The extensional component of the bulk strain is manifested by the development of fault heaves (width h) between the segments. The most convenient map-based measure of the fault-accommodated extension is the change in the effective width of the segments. This can be measured in Fig. 5a by the width of the segment plus the heave ($k = w + h$) expressed as a proportion of the original width (w). This proportion is here termed the apparent stretch $S^* = h/w$. It differs from a true stretch because it neglects the initially small component of strike-slip motion along the faults.

To retain approximate compatibility along the shear-zone boundary it is assumed that the segments shorten by folding, with fold hinges oriented perpendicular to the lengths of the segments. For simple shear (ideal strike-slip), which conserves area, the stretch resulting from folding along the segment lengths (here termed S') is the reciprocal of S^*. Fig. 5b shows how approximate strain compatibility can be maintained across a zone of heterogeneous simple shear, where fault strikes and apparent stretch vary across the zone.

For the simple shear case (ideal strike-slip), the apparent stretch S^* can be shown (Fig. 5c and Appendix A) to be

$$S^* = 1/\sqrt{1 - \gamma + \gamma^2/2}. \quad (1)$$

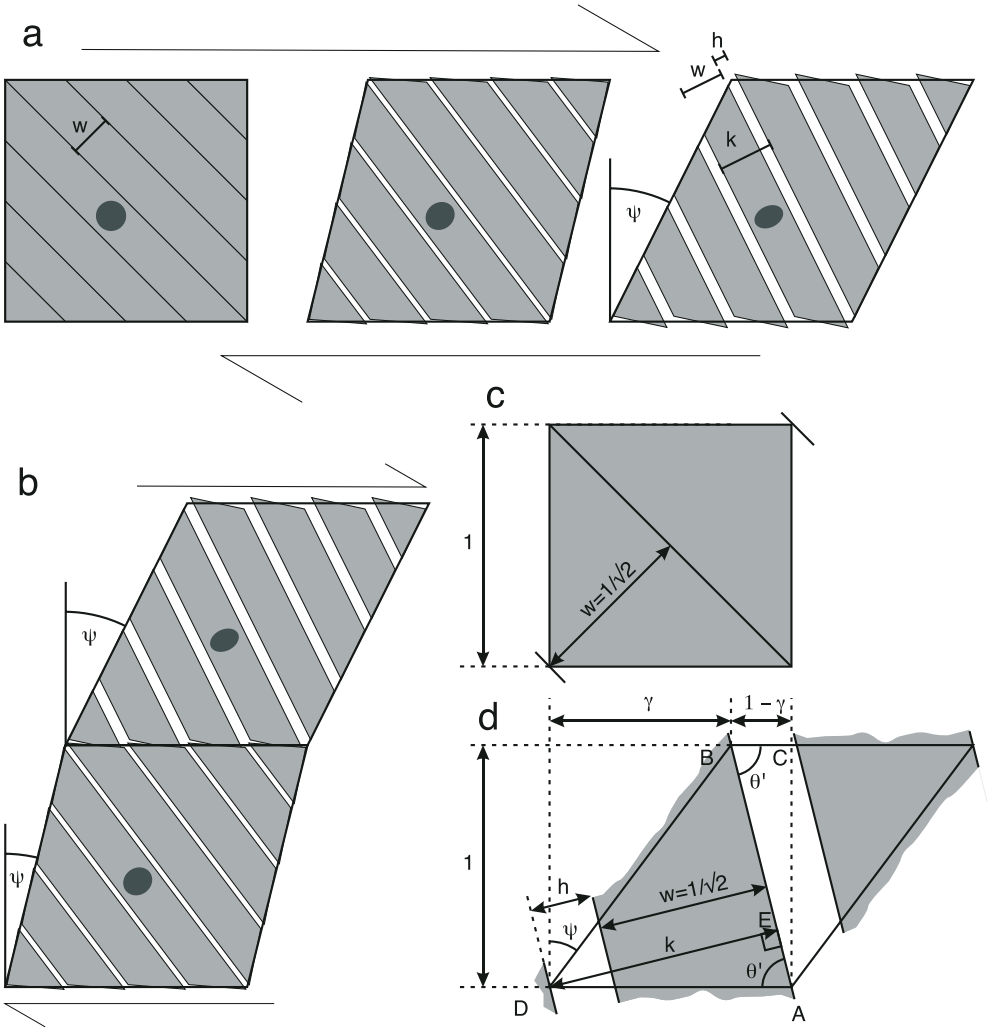

Fig. 5. Constructions for the strike-slip (simple shear) case. (a) Diagram showing progressive deformation in simple shear, with extensional component of strain accommodated by faults. (b) Modification to show heterogeneous simple shear. (c) Small unit square region containing a single extensional fault. (d) Unit square after deformation, showing quantities referred to in text and Appendix A.

Fig. 6 graphs the relationship between S^* and shear strain γ, and between S^* and angle of shear ψ. Notice that S^* increases to a maximum when $\gamma = 1$ ($\psi = 45°$), where the fault segments are perpendicular to the shear zone boundary. Beyond this point, further deformation leads to progressive closing of the fault heaves as the normal faults become inverted. Beyond $\gamma = 2$ ($\psi = 63.4°$) the originally normal faults are completely inverted and acquire reverse offsets as S^* falls below unity.

4. Kinematic model for transtension (arbitrary initial fault orientation)

4.1. General characteristics of transtension model

Now consider the general case of a transtensional finite strain. In this case there will be a component of extension perpendicular to the shear zone boundary, and the initial orientation of faults cannot be assumed to be at 45° to the boundary. Although many different shapes of incremental strain ellipsoid can be considered (e.g. Fossen and Tikoff, 1998), the most likely type of bulk strain at a releasing bend in a strike-slip boundary is illustrated in Fig. 7a, where a basin is developed between two otherwise rigid blocks. In this case, the short segment of fault that forms the basin boundary (horizontal in Fig. 7a) will represent a unique horizontal line of no extension. This type of transtensional strain corresponds to the kinematics of Sanderson and Marchini (1984), and to case B in the range of possibilities considered by Fossen and Tikoff (Fossen and Tikoff, 1998).

In general, the orientation of the extension axis will not be perpendicular to any of the basin boundaries, so faults developed within the basin will have different orientations from the basin boundaries. Initially, the case of arbitrarily oriented pre-existing faults will be considered, with strike θ

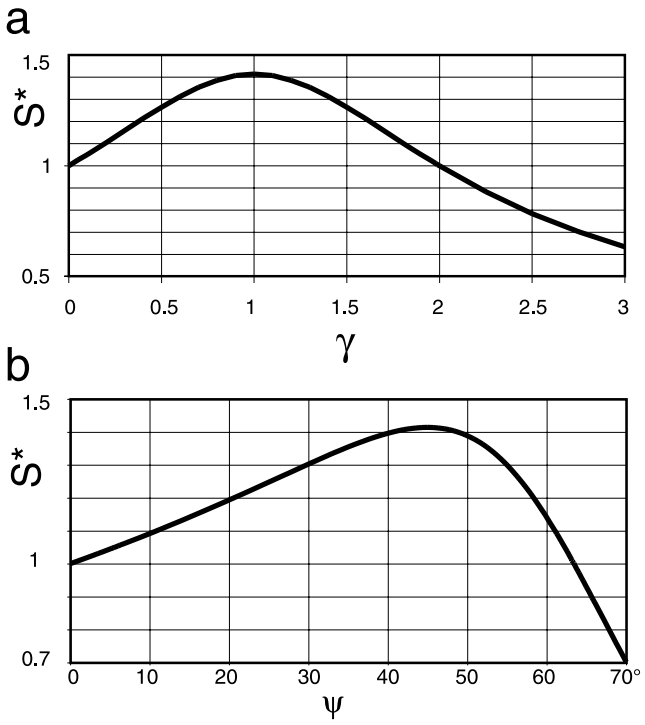

Fig. 6. Graphs for the case of ideal strike-slip (simple shear). Top: graph of apparent stretch against shear strain γ. Bottom: graph of apparent stretch against angle of shear ψ.

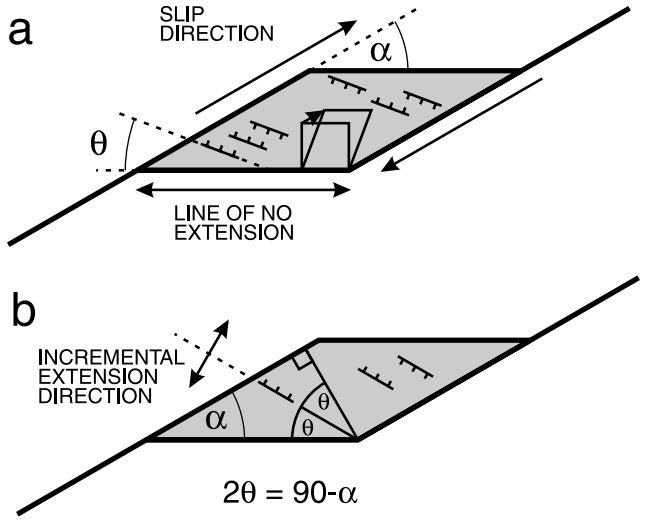

Fig. 7. Diagrams illustrating the general case of transtension. (a) Diagram showing slip direction and distortion of a unit square in a generalized pull-apart basin at a releasing bend. Extensional faults within the basin are oriented at an arbitrary angle θ. (b) Diagram showing angular relationships where extensional faults are oriented perpendicular to the incremental stretching direction.

clockwise from the shear zone boundary (Fig. 7a). In a later section, θ will be constrained to be perpendicular to an instantaneous extension axis consistent with progressive transtension.

4.2. Kinematic model for transtension

Consider the finite strain as due to a simple shear with shear strain T parallel to the x-axis (shear zone boundary), followed by a stretch S perpendicular to this line. The two-dimensional deformation gradient tensor describing this strain is:

$$\begin{pmatrix} 1 & T \\ 0 & S \end{pmatrix}$$

The final value of the shear strain along the zone

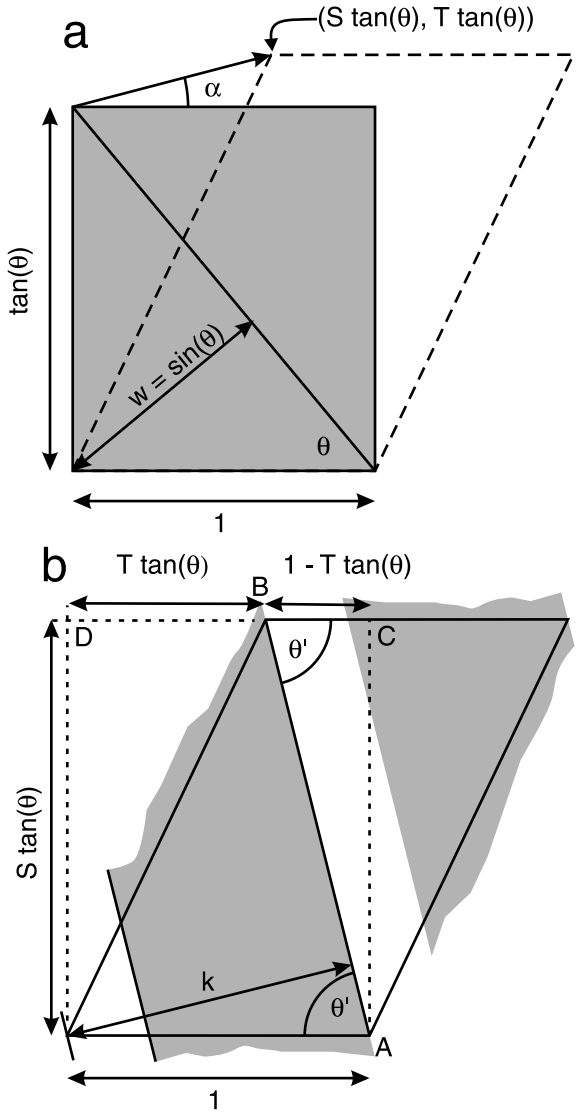

Fig. 8. Construction equivalent to Fig. 5, but drawn for the general case of transtension. (a) Small rectangular element of unit width cut by a single extensional fault. (b) Rectangular element after deformation, showing quantities referred to in text and Appendices B–D.

boundary is $\gamma = T/S$. A convenient measure of the amount of extension relative to strike-slip shear is designated $A = (S-1)/T$. The displacement direction (counterclockwise from the zone boundary) of particles is given by α, where $\tan\alpha = A$.

These quantities are shown in Fig. 8 for a small, initially rectangular element with unit extent measured parallel to the shear zone boundary, diagonally transected by a single fault. The initial height of the element (perpendicular to the shear zone boundary) is $\tan\theta$. The initial width of a single fault block $w = \sin\theta$.

After deformation the fault is rotated to orientation θ'. The apparent stretch S^* is shown in Appendix B to be given by:

$$\frac{1}{S^{*2}} = \sin^2\theta + \frac{1}{S^2}(\cos\theta - T\sin\theta)^2 \tag{2}$$

For a given α we can write $\tan\alpha = (S-1)/T$ whence $T = (S-1)/\tan\alpha$. Substituting for T in Eq. (2) gives the relationship of S^* to S and α:

$$\frac{1}{S^{*2}} = \sin^2\theta + \frac{1}{S^2}\left(\cos\theta + \frac{(1-S)\sin\theta}{\tan\alpha}\right)^2 \tag{3}$$

4.3. Determination of transtension parameters from measurements of deformed basins

In a given basin we are unlikely to be able obtain a direct estimate of S or T; however, the final orientation θ' of faults may be known, and it may be possible to measure, from maps and cross-sections, the apparent stretches S^* and S' across and along the fault segments, respectively. We can therefore attempt to obtain estimates of α, S, T, and θ, using observed values of independently determined S^* , S', and θ'.

The values S, T, θ, and α can be obtained as shown in Appendix B:

$$S = S^* S'. \tag{4}$$

$$\sin\theta = \sin\theta'/S^* \tag{5}$$

$$T = \cot\theta - S\cot\theta' \tag{6}$$

$$\tan\alpha = (S-1)/T \tag{7}$$

4.4. Application to Stellarton example

These relationships allow us to explore the role of simple shear and transtension for the map-scale faulting and folding exhibited by the Foord seam in the Stellarton Basin. Strain within the area of Fig. 2b is significantly heterogeneous, as indicated by the northward widening of fault heaves. However, estimates of the apparent stretch can be obtained in the regularly faulted area around the Albion syncline, where along-segment shortening is taken up by folding. A dashed line marks the approximate south limit of faulting, and is roughly parallel to an inferred basin margin that lay to the southwest (now removed by erosion). This line is taken as the orientation of the shear-zone boundary. Sections A–A′ and B–B′, drawn perpendicular to faults, show apparent stretches (S^*) of ~1.14. Sections drawn parallel to the faults (C–C′ to E–E′, Fig. 2) show shortening by folding, with an apparent stretch of ~0.9. Although there is some indication in the Stellarton basin that folding may have continued after faulting (Waldron, 2004), we here assume that both were part of a single strain history, and examine the resulting bulk strain. Hence, we calculate S to be 1.015 (Eq. (4)). The measured value of θ' is ~48° (Fig. 2), whence θ is calculated to be 41°. The value of T is estimated at 0.24, and α is 6°. This value is insensitive to the estimated orientation of the shear zone boundary (the grey dashed line in Fig. 2b); variations of up to 10° in θ' produce values of α that are effectively identical.

Thus, the observed map-scale deformation of the Foord seam in the Stellarton basin can be accounted for by a bulk strain that departs only slightly from dextral simple shear. In the portion of Fig. 2b that contains the cross-sections, the faults and intervening fault blocks are estimated to have been rotated about 7° clockwise during this strain, from an original orientation that was approximately NNW. Fig. 9 shows a schematic retro-deformation, indicating how this strain affected the seam.

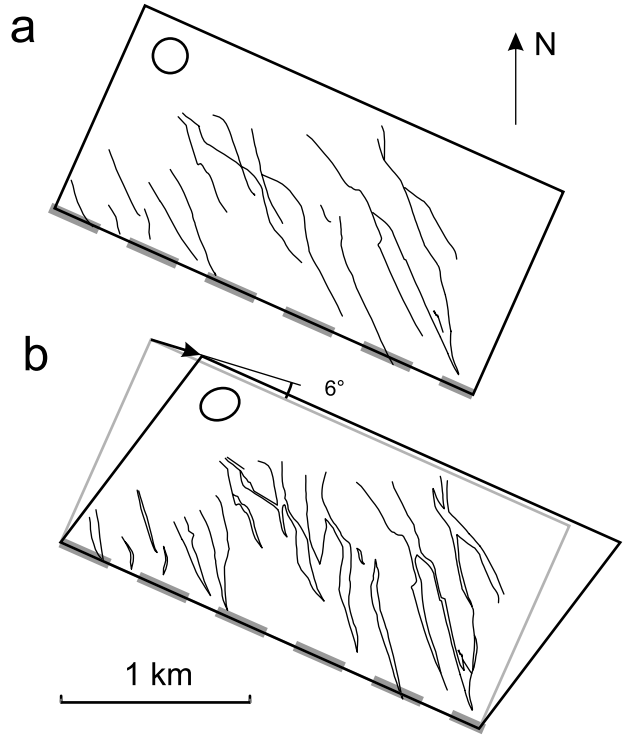

Fig. 9. (a) Schematic retro-deformed map of the Foord seam (area shown in Fig. 2b), showing general orientation of faults at the start of deformation. (b) Simplified present-day map of faults, with strain ellipse showing the distortion required to account for distribution of fault heaves. Large parallelogram represents distorted version of rectangle in (a). Divergence α of slip direction (arrow) from shear zone boundary (dashed grey line) is 6°.

5. Transtension (faults initiated perpendicular to incremental extension)

5.1. Initial fault orientation

The above relationships apply to finite transtension accommodated on arbitrarily oriented faults However, if it is assumed that faults are initiated as a result of transtensional strain then the angle θ is dependent (Appendix C) on the value of A, such that $\tan(2\theta) = 1/A$, and

$$2\theta = 90 - \alpha. \tag{8}$$

This results in the geometry shown in Fig. 7b. Note that if either α or θ is known, then the other can be found by a simple right-triangle construction.

5.2. Effect of transtension on structures

Substituting for θ in Eq. (3) above, it can be shown (Appendix D) that

$$\frac{2}{S^{*2}} = 1 - \sin\alpha + \frac{1 + T^2 - 2T\cos\alpha(1 - T^2)\sin\alpha}{(1 + T\tan\alpha)^2} \tag{9}$$

Apparent stretch S^* varies with shear T, for various values of α, as shown in Fig. 10a. At low values of α (representing dominantly strike-slip transtension), the apparent stretch will increase to a maximum and then decrease again as initially extensional faults are inverted in compression. For extension-dominated transtension, with values of α above about 40°, initially extensional faults do not invert in compression in the range of T shown in Fig. 10a.

A further condition limits the applicability of the graphs in Fig. 10. If the amount of extension (relative to shear) is large, then the strain *along* the fault-bounded blocks is extensional also. Under these circumstances, all horizontal directions within the basin suffer extension. Additional orientations of normal faults might be expected to develop to accommodate this extension, and simple models of rotating fault blocks become inapplicable. The limiting condition for extension along the fault blocks is shown by a bold grey line ($S' = 1.0$) in Fig. 10; only the area below this boundary represents conditions that satisfy the initial assumptions of the model. Other lines in Fig. 10a mark the conditions where S' is slightly lower and higher than unity, to illustrate the amounts of along-block strain that would be predicted.

Fig. 10a serves for predicting the behaviour of a transtensional basin of known angle of extension α and shear T. For the interpretation of observations from naturally occurring basins, it is more likely that apparent stretch S^* and fault orientation θ' will be measurable quantities. Accordingly, Fig. 10b graphs S^* against θ', and shows curves for values of T and α. Once again, practical

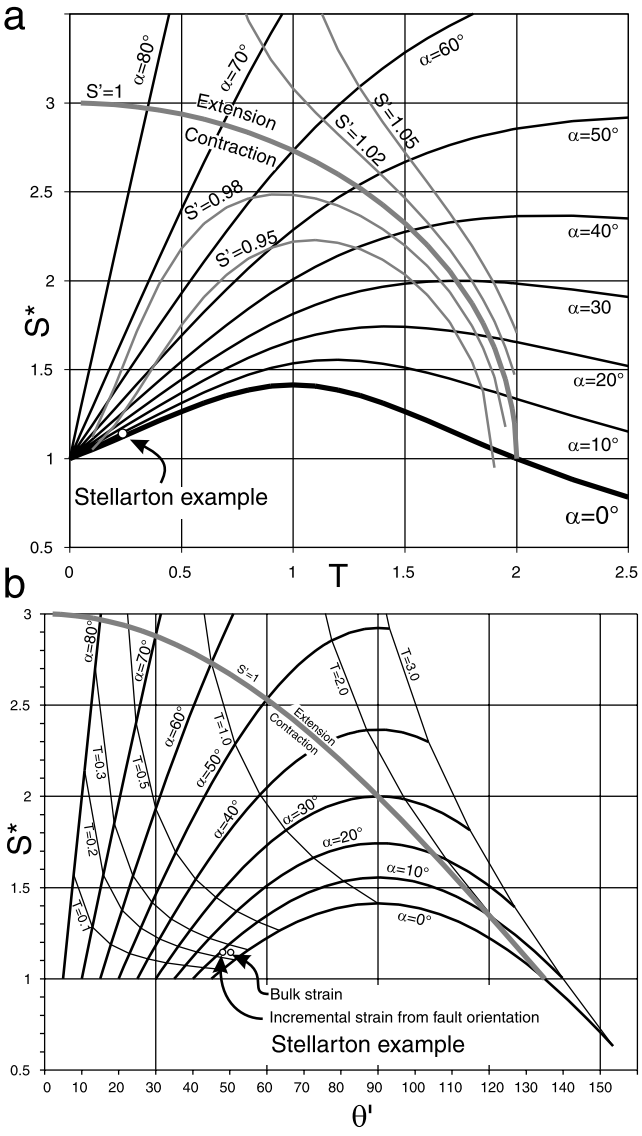

Fig. 10. Graphs for progressive transtension in which faults are initiated perpendicular to maximum incremental extension. In each graph a bold grey line ($S' = 1.0$) separates a region where there is shortening in some directions within the plane, from a region (above the line) where all lines within the plane are extended, and multiple orientations of faults would be expected. (a) Graph of apparent stretch S^* against shear strain component T. (b) Graph of S^* against final fault orientation θ'. Points marked in (b) show (i) the bulk strain affecting the Foord seam at Stellarton, based on estimates of S^* and S', and (ii) the incremental strain, based on estimates of S^* and θ'.

use of the graph is limited to cases where S' is less than or equal to unity (below the bold grey line labelled $S' = 1.0$).

5.3. Application to Stellarton example

These relationships can now be used to determine whether the initial orientations of faults in the Stellarton example were controlled by the same type of strain that produced the overall distortion described in the previous section. This is most easily accomplished using the simple relationship of Eq. (8): $2\theta = 90 - \alpha$. The geometry shown in

Fig. 2b corresponds to a θ value of 41°, whence α is predicted to be 8°. This compares closely with the calculated value of 6°, but suggests a slightly larger extensional component in the incremental strain at the time of fault initiation than in the overall bulk strain, consistent with the field evidence suggesting a change from transtension to transpression late in the deformation history. The two estimates cannot be separated on a plot of S^* against T (Fig. 10a) though they are just distinguishable in the plot of S^* against θ' shown in Fig. 10b. It should be noted that when θ' is used in this way to constrain α, the results are much more sensitive to errors in the determination of the orientation of the shear zone boundary (the dashed grey line in Fig. 2b). A 5° error in θ' leads to a change in α of $\sim$8°.

6. Discussion

In a previous account of the development of the Stellarton basin (Waldron, 2004), it was inferred that basin extension was controlled primarily by strike-slip motion parallel to the Cobequid Fault (Fig. 2), which strikes approximately east–west. In this context, the angular relationships described above and shown in Fig. 2 are somewhat unexpected, because east–west slip would have resulted in a value of $\alpha = 24°$, rather than the 6–8° values estimated. A number of explanations are possible. First, it is clear that the faults in the Foord seam represent only a small part of the deformation history of the basin, soon after deposition of the Foord seam, and they may reflect an interval of near-simple-shear occurring at this time. Second, only faults apparent in mine plans were included in the analysis; typically these are faults with sufficient throw to affect mining operations. Outcrop observations (Waldron, 2004) show that small-scale extensional faults are common, and therefore that the apparent stretch may be underestimated. Fig. 10b indicates, however, that a much larger apparent stretch, in the order of 1.35, accompanied by more rotation of faults, would have been required for east–west slip with $\alpha = 24°$.

7. Conclusions

The model developed here is clearly a simplification of the behaviour of real strike-slip and transtensional basins. However, unlike many previous models, it recognizes the progressive nature, and in particular, the rotational component, of the strain that affects such basins in map view, which has been neglected in many previous accounts. The relationships derived here show that for a simple scenario, involving a basin in uniform transtension with no extension parallel to a shear-zone boundary, there is a straightforward relationship between strain and fault orientation. Observations of apparent stretch, across multiple normal faults, are important for understanding the history of pull-apart basins. Although not clearly available for the published examples shown in Fig. 3, these measurements should be easy to make in basins that have been explored using (especially) 3-D seismic techniques, and will allow quantification of the deformation of such basins.

Acknowledgements

Initial work on the Stellarton basin was supported by the Geological Survey of Canada through a Supply and Services Canada contract with Saint Mary's University. Preparation of the paper was assisted by NSERC Discovery Grant A8508. Data on Stellarton were compiled with the assistance of Kevin Gillis and the Nova Scotia Department of Natural Resources. James Bradley assisted with measurements and data from the Stellarton basin. I acknowledge a useful discussion with John Dewey on basin kinematics. Journal reviewers Nigel Woodcock and Gregor Schoenborn, and editor David Ferrill, provided helpful and encouraging comments.

Appendix A. Value of apparent stretch in simple shear

Consider the unit square shown in Fig. 5c, divided by a single extensional fault into two triangular segments. The initial width of the segments is given by $w = 1/\sqrt{2}$. The square is subjected to simple shear through an angle ψ, producing a shear strain $\gamma = \tan(\psi)$ along the shear zone boundary (Fig. 5d).

The angle θ' that the segments make with the boundary, initially 45°, is increased to $\operatorname{arccot}(1-\gamma)$ as shown by triangle ABC in Fig. 5d. The combined width $k = h + w$ is given by triangle ADE, such that:

$$k = \sin\theta' = \sin(\operatorname{arccot}(1-\gamma)) = 1/\sqrt{2 - 2\gamma + \gamma^2}. \quad (10)$$

The apparent stretch S^* in this direction is then k/w or

$$S^* = 1/\sqrt{1 + \gamma + \gamma^2/2}. \quad (11)$$

Appendix B. Apparent stretch in transtension (arbitrary initial fault orientation)

Consider the small rectangular element with unit length, measured parallel to the shear zone boundary, as shown in Fig. 8, diagonally transected by a fault, orientation θ. The initial width of the element (perpendicular to the shear zone boundary) is $\tan\theta$. The initial width of a single fault block $w = \sin\theta$.

After deformation the fault is rotated to orientation θ'. The effective new width of the segment $k = \sin\theta'$.

In this case the apparent stretch is:

$$S^* = \sin\theta'/\sin\theta \quad (12)$$

However, k can be expressed in terms of θ because, as shown in Fig. 8, triangle ABC:

$$\tan\theta' = \frac{S\tan\theta}{1 - T\tan\theta} = \frac{S}{\cot\theta - T}$$

Hence:

$$\sin\theta' = \frac{1}{\sqrt{1 + \frac{1}{S^2}(\cot\theta - T)^2}}$$

So:

$$S^* = \sin\theta'/\sin\theta = \frac{1}{\sin\theta\sqrt{1 + \frac{1}{S^2}(\cot\theta - T)^2}}$$

$$= \frac{1}{\sqrt{\sin^2\theta + \frac{1}{S^2}(\cos\theta - T\sin\theta)^2}}$$

or, alternatively:

$$\frac{1}{S^{*2}} = \sin^2\theta + \frac{1}{S^2}(\cos\theta - T\sin\theta)^2 \tag{13}$$

For the simple shear case described in the previous section, $T=\gamma$, $S=1$, $\theta=45°$ and $\alpha=0$. This expression reduces to $S^* = 1/\sqrt{(1-\gamma+\gamma^2/2)}$ as above.

For a given α we can write $\tan\alpha=(S-1)/T$ whence $T=(S-1)/\tan\alpha$. Substituting for T in Eq. (7) gives the relationship of S^* to S and α:

$$\frac{1}{S^{*2}} = \sin^2\theta + \frac{1}{S^2}\left(\cos\theta + \frac{(1-S)\sin\theta}{\tan\alpha}\right)^2 \tag{14}$$

Typically S^*, S' and θ' may be determined from measurement; the values of S, T, θ, and α can be found as follows.

The area change involved in the strain shown in Fig. 8 is simply S (because the longitudinal strain along the shear zone boundary is assumed to be one). Hence:

$$S = S^* S'. \tag{15}$$

To find θ, rearrange Eq. (3) above:

$$\sin\theta = \sin\theta'/S^* \tag{16}$$

To find T, note (Fig. 8) that:

$$\mathrm{BC} = S\tan\theta\cot\theta'.$$

Hence:

$$\mathrm{BD} = 1 - S\tan\theta\cot\theta'.$$

But this length is already known to equal $T\tan\theta$, so:

$$T\tan\theta = 1 - S\tan\theta\cot\theta'$$

whence

$$T = \cot\theta - S\cot\theta' \tag{17}$$

Finally, from the definition of α

$$\tan\alpha = (S-1)/T \tag{18}$$

Appendix C. Transtension: fault initiation perpendicular to instantaneous extension

In a basin filled with uniform sediment undergoing transtension, the orientation of faults is likely to be controlled by the orientations of the incremental strain axes.

To determine these orientations consider first the finite strain axes for a strain defined by the deformation gradient tensor:

$$\begin{pmatrix} 1 & T \\ 0 & S \end{pmatrix}$$

The finite strain axes are oriented (Ramsay and Huber, 1983) at angles θ', measured counterclockwise from the x-axis, such that:

$$\tan(2\theta') = 2TS/(1 + T^2 - S^2) \tag{19}$$

or, substituting $1+AT$ for S, and converting to the clockwise convention of Fig. 8:

$$\tan(2\theta') = \frac{-2(T + AT^2)}{T^2(1 + A^2) - 2AT}$$

We assume that faults form with orientation θ in response to a small incremental strain, perpendicular to the incremental extension axis. Under these circumstances, T tends to zero. Hence:

$$\tan(2\theta) = 1/A = T(S-1) \tag{20}$$

The same result can be obtained by equating the infinitesimal strain and stress tensors, and locating the stress axes.

This expression has solutions spaced at 90°, corresponding to the orientations of strain axes. For transtension, the lower value of θ corresponds to the initial orientation of normal faults formed perpendicular to the extension direction.

Because $A=\tan\alpha$, there is a simple relationship between θ and α:

$$2\theta = 90 - \alpha \tag{21}$$

Appendix D. Relationship between S*, T and α

In this section, the expression for θ (Appendix C) is substituted into the equation for S^* derived in Appendix B. To simplify the formulas, a quantity α' is defined as $90°-\alpha$, so $\theta=\alpha'/2$. Substituting this into Eq. (7) gives:

$$\frac{1}{S^{*2}} = \sin^2\left(\frac{\alpha'}{2}\right) + \frac{1}{S^2}\left(\cos\left(\frac{\alpha'}{2}\right) - T\sin\left(\frac{\alpha'}{2}\right)\right)^2 \tag{22}$$

Half-angle formulas allow this to be expressed as

$$\frac{1}{S^{*2}} = \left(\frac{1-\cos\alpha'}{2}\right) + \frac{1}{S^2}\left(\sqrt{\frac{1+\cos\alpha'}{2}} - T\sqrt{\frac{1-\cos\alpha'}{2}}\right)^2$$

whence

$$\frac{2}{S^{*2}} = 1-\cos\alpha' + \frac{1}{S^2}\left(\sqrt{1+\cos\alpha'} - T\sqrt{1-\cos\alpha'}\right)^2.$$

Expanding the right-hand side yields:

$$\frac{2}{S^{*2}} = 1-\cos\alpha' + \frac{1}{S^2}\left(1+\cos\alpha' - 2T\sqrt{1-\cos^2\alpha'} + T^2(1-\cos\alpha')\right)$$

Substituting functions of α then gives:

$$\frac{2}{S^{*2}} = 1-\sin\alpha + \frac{1}{S^2}\left(1+\sin\alpha - 2T\cos\alpha + T^2(1-\sin\alpha)\right)$$

$$\frac{2}{S^{*2}} = 1-\sin\alpha + \frac{1}{S^2}\left(1+T^2 - 2T\cos\alpha + (1-T^2)\sin\alpha\right) \quad (23)$$

Then, because $S = T\tan(\alpha)+1$, S^* can be expressed purely in terms of α and T as follows:

$$\frac{2}{S^{*2}} = 1-\sin\alpha + \frac{1+T^2-2T\cos\alpha+(1-T^2)\sin\alpha}{(1+T\tan\alpha)^2} \quad (24)$$

References

Allen, M.B., MacDonald, D.I.M., Xun, Z., Vincent, S.J., Brouet-Menzies, C., 1998. Transtensional deformation in the evolution of the Bohai Basin, northern China, in: Holdsworth, R.E., Strachan, R.A., Dewey, J.F. (Eds.), Continental Transpressional and Transtensional Tectonics. Geological Society of London Special Publication, 135, pp. 215–229.

Aydin, A., Nur, A., 1985. The types and role of stepovers in strike-slip tectonics, in: Biddle, K.T., Christie-Blick, N. (Eds.), Strike-slip Deformation, Basin Formation, and Sedimentation. Society of Economic Paleontologists and Mineralogists Special Publication, 37, pp. 35–44.

Cemen, I., Wright, L.A., Drake, R.E., Johnson, F.C., 1985. Cenozoic sedimentation and sequence of deformational events at the southeastern end of the Furnace Creek strike-slip fault zone, Death Valley region, California, in: Biddle, K.T., Christie-Blick, N. (Eds.), Strike-slip Deformation, Basin Formation, and Sedimentation. Society of Economic Paleontologists and Mineralogists Special Publication, 37, pp. 127–141.

Christie-Blick, N., Biddle, K.T., 1985. Deformation and basin formation along strike-slip faults, in: Biddle, K.T., Christie-Blick, N. (Eds.), Strike-slip Deformation, Basin Formation, and Sedimentation. Society of Economic Paleontologists and Mineralogists Special Publication, 37, pp. 1–34.

Dewey, J.F., 2002. Transtension in arcs and orogens. International Geology Review 44, 402–439.

Dibblee, T.W., 1977. Strike-slip tectonics of the San Andreas Fault and its role in Cenozoic basin evolvement, in: Sylvester, A.G. (Ed.), Wrench Fault Tectonics American Association of Petroleum Geologists Reprint Series, 28, pp. 159–172.

Dokka, R.K., Ross, T.M., Lu, G., 1998. The Trans Mojave–Sierran shear zone and its role in Early Miocene collapse of southwestern North America, in: Holdsworth, R.E., Strachan, R.A., Dewey, J.F. (Eds.), Continental Transpressional and Transtensional Tectonics. Geological Society of London Special Publication, 135, pp. 183–202.

Dooley, T., McClay, K., 1997. Analog modeling of pull-apart basins. American Association of Petroleum Geologists Bulletin 81, 1804–1826.

Fossen, H., Tikoff, B., 1998. Extended models of transpression and transtension, and application to tectonic settings, in: Holdsworth, R.E., Strachan, R.A., Dewey, J.F. (Eds.), Continental Transpressional and Transtensional Tectonics. Geological Society of London Special Publication, 135, pp. 15–33.

Garfunkel, Z., 1974. Model for the late Cenozoic tectonic history of the Mojave desert, California, and for its relation to adjacent areas. Geological Society of America Bulletin 85, 1931–1944.

Garfunkel, Z., Ron, H., 1985. Block rotation and deformation by strike-slip faults. Journal of Geophysical Research 90, 8589–8602.

Harding, T.P., 1974. Petroleum traps associated with wrench faults. American Association of Petroleum Geologists Bulletin 58, 1290–1304.

Harding, T.P., Vierbuchen, R.C., Christie-Blick, N., 1985. Structural styles, plate tectonic settings, and hydrocarbon potential of divergent (transtensional) wrench faults, in: Biddle, K.T., Christie-Blick, N. (Eds.), Strike-slip Deformation, Basin Formation, and Sedimentation. Society of Economic Paleontologists and Mineralogists Special Publication, 37, pp. 51–77.

Rahe, B., Ferrill, D.A., Morris, A.P., 1998. Physical analog modeling of pull-apart basin evolution. Tectonophysics 285, 21–40.

Ramsay, J.G., Huber, M.I., 1983. The Techniques of Modern Structural Geology. Volume 2: Folds and Fractures. Academic Press, London.

Rodgers, D.A., 1980. Analysis of pull-apart basin development produced by en echelon strike-slip faults, in: Ballance, P.F., Reading, H.G. (Eds.), Sedimentation in Oblique-Slip Mobile Zones. International Association of Sedimentologists Special Publication, 4, pp. 27–41.

Sanderson, D.J., Marchini, W., 1984. Transpression. Journal of Structural Geology 6, 111–117.

Sims, D., Ferrill, D.A., Stamatakos, J.A., 1999. Role of a ductile decollement in the development of pull-apart basins: experimental results and natural examples. Journal of Structural Geology 21, 533–554.

Waldron, J.W.F., 2004. Anatomy and evolution of a pull-apart basin, Stellarton, Nova Scotia. Geological Society of America Bulletin 116, 109–127.

Wood, R.A., Pettinga, J.R., Bannister, S., Lamarche, G., McMorran, T.J., 1994. Structure of the Hanmer strike-slip basin, Hope fault, New Zealand. Geological Society of America Bulletin 106, 1459–1473.

Woodcock, N.H., Fischer, M., 1986. Strike-slip duplexes. Journal of Structural Geology 8 (7), 725–735.

Yeo, G.M., Gao, R.-X., 1987. Stellarton graben: an upper Carboniferous pull-apart basin in northern Nova Scotia, in: Beaumont, C., Tankard, A.J. (Eds.), Sedimentary Basins and Basin-Forming Mechanisms. Canadian Society of Petroleum Geologists Memoir, 12, pp. 299–309.